Xenics Infrared Solutions

Fire detection

Archeological Treasures Protection based on early Forest Wildfire Multi Band Imaging Detection System.

B.Gouverneur[1*], S.Verstockt[2], E.Pauwels[3], J. Han[3], P.M. de Zeeuw[3], J.Vermeiren[1]
[1]Xenics nv Ambachtenlaan 44 BE-3001 Leuven, Belgium
[2]Multimedia Lab, Ghent IBBT, Gaston Crommenlaan 8, bus 201, B-9050 Ledeberg Ghent, Belgium
[3]Centrum Wiskunde & Informatica, P.O. Box 94079, NL-1090 GB, Asterdam, The Netherlands

ABSTRACT

Various visible and infrared cameras have been tested for the early detection of wildfires to protect archeological treasures. This analysis was possible thanks to the EU Firesense project (FP7-244088). Although visible cameras are low cost and give good results during daytime for smoke detection, they fall short under bad visibility conditions. In order to improve the fire detection probability and reduce the false alarms, several infrared bands are tested ranging from the NIR to the LWIR. The SWIR and the LWIR band are helpful to locate the fire through smoke if there is a direct Line Of Sight. The Emphasis is also put on the physical and the electro-optical system modeling for forest fire detection at short and longer ranges. The fusion in three bands (Visible, SWIR, LWIR) is discussed at the pixel level for image enhancement and for fire detection.

Keywords: Multiband Electro-Optical System, Forest Fire, Cultural Heritage, Sensor Fusion, Fire Detection Modeling.

1. INTRODUCTION

Most of the efforts in early detection of wildfires, particularly around the precious cultural heritage sites in the Mediterranean area, are still done by human observers. Because this method is very labor intensive, the results are not very satisfactory, as the observers get tired and bored quickly. For this reason a lot of effort is spent to detect wildfires in an early stage by the processing of visible images. Smoke and direct fire detection have shown to yield excellent results both from the point of view of detection and false alarms. Unfortunately, the early detection of smoke works only during day time and when the wind is not too strong (dilution of the smoke), partly limiting the early detection capabilities.
For this reason, the Firesense consortium has decided to investigate other wavelength bands, which can potentially overcome the above cited limitations. The main candidates are the Infrared bands, as they allow detecting the emitted radiation and detecting radiation more at the emission peak of the spectrum.
The short wave infrared (SWIR) waveband ranges from [0.9 - 1.7 µm] or [0.9 – 2.5 µm] band, the middle wave infrared (MWIR) waveband from [3 - 5 µm] and the long wave infrared (LWIR) waveband from [8 - 12 µm], coinciding with the atmospheric transmission windows are studied in detail. Visible (color) cameras are very attractive to increase situational awareness and to carry out reliable smoke detections during day time operations. Smoke is often white due to humidity and is seen at the early stages of the fire even at long range. At short range, we are often able to see the flames. The flames are difficult to see at long range in the forest except if the fire is large. The LWIR camera is able to create a temperature map of the scene. The SWIR camera operates very close to the emission peak of the fire or hot ash, and has less influence from the solar irradiance. The LWIR and the SWIR are able to see through smoke; this is important in order to localize the fire and in order to conduct search and rescue operations. The MWIR band detector, finally, has very good detection properties for long range (5 to 15 km) observations above land.
Cost of implementation is an important factor for the roll-out of a fire detection system. Clearly, visible cameras are most cost effective, followed by uncooled LWIR and SWIR cameras. The pricing of cooled MWIR and LWIR makes them attractive for large scale deployment. We will present a simplified physical and electro-optical system model for fire detection.

* Benedict.gouverneur@xenics.com, Tel: +32 (0)16 38 99 00, Fax: +32 (0)16 38 99 01, http://www.xenics.com

2. FIRE DETECTION MODELING

The imaging sensors detect the direct radiation produced by the heat of the fire (hot ashes, flames and smoke) and the background (forest) as well as the reflected radiation from the sun and the fire. Before reaching the detector, the direct and reflected radiations are affected by the atmosphere, attenuating the radiation due to absorption and scattering. At long range, the omission of the atmospheric and emissivity fire modeling could be the origin of several errors.

2.1 Wood Ignition and Burning Process for Fire Detection Model

Knowing at which temperature or at which minimum flux the wood would (may) ignite will help us to define some values for early fire detection modeling. It is shown that wood will ignite with a minimal temperature around 250 ˚C or when the wood is exposed to a heat flux of at least 4.3 $kW.m^{-2}$ [1]. The solar radiation is around 1350 $W.m^{-2}$. Depending on the type of wood, the degree of humidity or the measuring methods, the results vary in literature between 250 ˚C to 530 ˚C concerning the temperature and between 4.3 $kW.m^{-2}$ and 40 $kW.m^{-2}$ concerning the flux. With this high temperature difference it should be easy to detect the heat if the emissivity of the igniting wood is high, if there is no occlusion by the vegetation, and if the hot spot has (is) more or less the size of a camera pixel.

The outcome of biomass combustion is charcoal, soot, ashes, H_2O and CO_2. The complete combustion produces only hot air, plasma, gases and ashes, whereas incomplete combustion produces hot air, plasma, gases, smoke, soot and vapors. The size of the smoke particles is an important parameter. The amount of smoke produced and the smoke particle size distribution defines the transparency, the reflectivity (visibility or light extinction) and the emissivity of the smoke. The particle size of smoke from burning wood varies between 0.5 and 5 µm [2]. The radiation, emitted by the flame, extends from the visible to the infrared radiation spectrum. The turbulent forest fire flames have a high luminosity due to the soot. Larger quantities of soot from the fire increase the emissivity. If the color is red or orange in the visible band, the temperature will reach 700 to 1200 ˚C.

Temperature and emissivity can fluctuate due the variability of the flame (wind, topography, vegetation type). The wavelength dependent extinction of the light on soot and smoke particles is based on the Beer-Lambert-Bouguer law:

$$I_\lambda = I_\lambda^0 \cdot e^{-K_m m L} = I_\lambda^0 \cdot e^{-KL} \qquad (1)$$

K: light extinction coefficient, m: mass concentration in gr, L: the optical path length.
The extinction coefficient per unit mass K_m depends on the particle size distribution and the optical properties (λ, n_r) [2].

$$K_m = \frac{3}{2\rho m} \int_{d_{min}}^{d_{max}} \frac{1}{d} \frac{\delta m}{\delta d} Q_{ext}(d/\lambda, n_r) \delta d \qquad (2)$$

Mass size distribution $\delta m/\delta d$, particle diameter to wavelength of light d/λ, ρ: particle density, n_r particle refractive index.

Hagglund and Persson [3] observed that in thin flames, we have a band emission mechanism due to the molecular vibration of the water and dioxide carbon hot gases. The band radiation is the dominant radiation above the radiation emitted by the soot particles. When the flames are thick the soot radiation contribution is higher than the gas band radiation.

2.2 Flame and Smoke Model

The spectral emission (sun, fire or background) is based on Planck radiation formula. For the gray body where $\varepsilon<1$ is the emissivity, we can write the following in terms of wavelength λ:

$$M_{BB}(T,\lambda) = \varepsilon(\lambda) M_{BB}(T,\lambda) = \varepsilon(\lambda) \cdot \frac{2\pi c^2}{\lambda^5} \cdot \frac{1}{e^{\frac{hc}{\lambda k T}} - 1} \quad W.m^{-2}.\mu m^{-1} \qquad (3)$$

The total radiated energy:

$$M_{BB}(T,\lambda) = \varepsilon(\lambda)\sigma T^4 \qquad (4)$$

Planck constant h, Boltzmann constant k and speed of light c are the three main physical constants.

For a diffusive surface:

$$L_{BB}(T,\lambda) = \varepsilon(\lambda)L_{BB}(T,\lambda) = \frac{\varepsilon(\lambda)}{\pi}\cdot\frac{2\pi c^2}{\lambda^5}\cdot\frac{1}{e^{\frac{hc}{\lambda kT}}-1}\ W\cdot m^{-2}\cdot\mu m^{-4}\cdot sr^{-1} \qquad (5)$$

The temperature of the flame defines Planck's curve shape. The flame emissivity can be estimated by using the Quintiere equation:

$$\varepsilon_f = 1 - e^{-a_f L} \qquad (6)$$

L is the flame thickness, a_f the absorption coefficient of the flame and ε_f flame emissivity.
The absorption coefficient is a measure of how easy it is for radiation to penetrate a flame. The flame absorption coefficient ranges typically from 0.1 to 1 m^{-1}. If the thickness of the flame is more than 2 meters, the emissivity is close to 1 [3]. For large fires, smoke can obscure the flame which can reduce the radiant heat flux to the surroundings. The heat flux is received at the camera at range r from the flame at temperature T. The heat flux is reduced by a factor F called configuration factor depending on the shape of the flame and the surroundings and by a factor O called occlusion.

$$M_f(\lambda_1,T,O,F) = \int_{\lambda_1}^{\lambda_2} O\cdot F\cdot\frac{1-e^{-a_f L}}{\pi}\cdot\frac{2\pi c^2}{\lambda^5}\cdot\frac{1}{e^{\frac{hc}{\lambda kT}}-1}d\lambda \qquad (7)$$

The heat flux received at the camera level is given by:

$$M_f = \varepsilon_f\cdot\sigma\cdot F\cdot T^4 \qquad (8)$$

Example: the heat flux due to radiation from a wood fuel flame 1 m tall, 0.5 m wide and 0.5 m thick, k is 0.5 m^{-1} , T1= 700 K, T2=1400 K. Based on the figure from F=0.02 for short ranges (it decreases with distance). From formula 6

$$\varepsilon_f = 1 - e^{-a_f L} = 0.22$$

Based on formula 8 the result will be:

$$M_f = \varepsilon_f\cdot\sigma\cdot F\cdot T_1^4 = 36\ W/m^2$$

$$M_f = \varepsilon_f\cdot\sigma\cdot F\cdot T_2^4 = 948\ W/m^2$$

The emissivity will be low if the flame is small. The form factor is small if the distance range is long. If we take into account the occlusion, we will have:

$$M_f = O\cdot\varepsilon_f\cdot\sigma\cdot F\cdot T^4 \qquad 0 \ll O\cdot\varepsilon_f\cdot F \ll 1$$

Let's assume later F=O=1. The radiometric (temperature, emission), spatial, temporal and spectral information of the fire is used for classification. The flame radiation includes hot gases and soot [3]:

$$M_f = M_s + M_g - M_{sg} = \varepsilon_s\cdot\sigma\cdot T^4 + \varepsilon_g\cdot\sigma\cdot T^4 - \varepsilon_{sg}\cdot\sigma\cdot T^4 \qquad (9)$$

M_f: flame radiation, M_s: soot radiation, M_g: gas radiation, ε_f: flame emissivity, ε_s: soot emissivity, ε_g: gas emissivity.

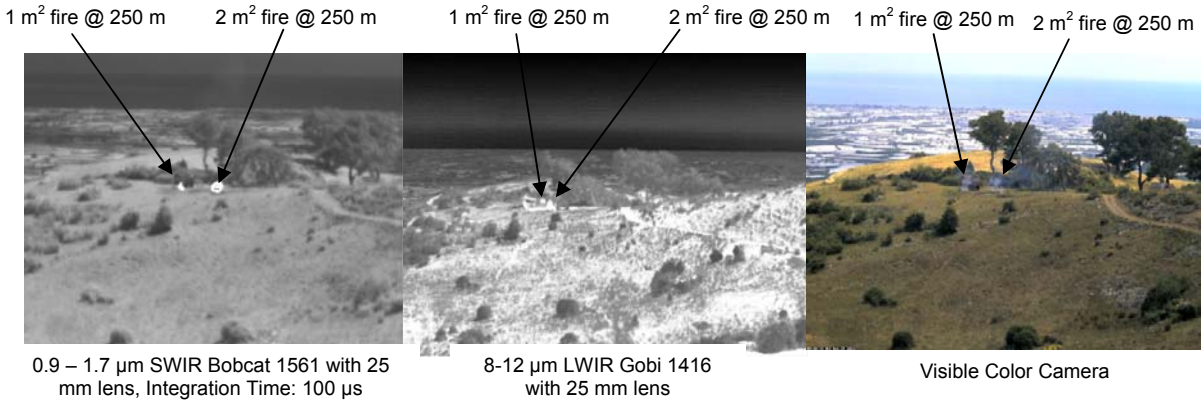

Figure 1: Two fires with smoke in the SWIR, LWIR and Visible WaveBands

The fire is optimally detected in the SWIR waveband (See Figure 1). The blob and fluctuating boundary of the white blob of the fire is well separated from the background. The smoke is not visible in SWIR, but is clearly visible in the visible waveband during the day. The LWIR fire blob is more difficult to detect due to background radiation during hot weather. The fluctuating flame and part of the fluctuating smoke is visible in the LWIR. An uncooled LWIR Micro-Bolometer camera could differentiate the fire radiation from the background radiation if the dynamic range of the signal of the sensor is high.

2.3 Gas Model

We saw that combustion gases (water and carbon dioxide mainly) radiate at distinct wavelength bands and soot radiates continuously. The emissivity of both gases is:

$$\varepsilon_g = \varepsilon_{H_2O} + \varepsilon_{CO_2} + \text{overlap correction} \qquad (10)$$

The emissivity of the gas is given by:

$$\varepsilon_g = 1 - e^{[-K_g pL]} \qquad (11)$$

K_g is the absorption coefficient ($m^{-1}atm^{-1}$), p is the partial pressure (atm) of the absorbing gas and L is the beam length. The total emissivity of the gases is a mixture of the different gases:

$$\varepsilon_g = \sum_{i=1}^{N} a_{g,i}\left[1 - e^{[-K_{g,i}(pL)]}\right] \quad \text{and} \quad \sum_{i=1}^{N} a_{g,i} = 1 \qquad (12)$$

Emissivity cannot be greater than 1.

The fire gases molecules (water, carbon dioxide) and the atmosphere gases molecules have infrared resonances that give rise to absorption lines (atmospheric gases at normal temperatures) and emission lines (fire and smoke gases at high temperatures). The absorption lines of the gases can be described with the absorption coefficient α(λ). The absorption and the emission measured by the thermal camera depend on the temperature of the gas T_g and the absorption coefficient [5].

$$L_\lambda(\lambda, T) = \exp[-\alpha(\lambda)l]L(\lambda, T) + [1 - \exp[-\alpha(\lambda)l]]L_\lambda(\lambda, T_g) \qquad (13)$$

The first term is the radiation loss of the target due to absorption and the second term is the radiation gained by the emission. If the absorption is low or the path length is low we will have, thanks to Taylor Series approximation:

$$L_\lambda(\lambda,T) = [1-\alpha(\lambda)]L(\lambda,T) + \alpha(\lambda)\varepsilon L_\lambda(\lambda,T_a) = L(\lambda,T) - \alpha(\lambda)\varepsilon(\lambda,T) + \alpha(\lambda)\varepsilon L_\lambda(\lambda,T_a) \quad (14)$$

For a short optical atmospheric length l the radiance of the fire measured by the thermal detector distance l over the spectral responsivity R(λ) is:

$$S = \int_0^\infty R(\lambda)L_\lambda(\lambda,T_a)d\lambda - l\int_0^\infty R(\lambda)\alpha(\lambda)L_\lambda(\lambda,T_a)d\lambda + l\int_0^\infty R(\lambda)\alpha(\lambda)L_\lambda(\lambda,T_a)d\lambda \quad (15)$$

The first term is the signal from any atmospheric interaction. The second term is the decrease of the signal due to gas absorption. The third term is the increase of signal due to the gas radiation.

2.4 Reflected Radiation Model

With the Kirchhoff law the incident radiation is absorbed, reflected or transmitted α+ρ+τ=1. If the object is opaque, τ=0, α=ε and ε+ρ=1. The emissivity and the reflectivity are complementary (ε=1-ρ).

The left image of Figure 2 is captured from an [8-12 µm] bolometer. The temperature and emissivity of the wood pile is high. The emissivity of the flame in the LWIR is lower and the transmission part is higher (part of the background is seen through the flame). The ice and water have low emissivity. The reflection portion will be higher. The effect will be the same in a forest. All non-blackbody objects (objects with ε<1) both reflect and emit radiation. If the background has an emissivity of 80%, it will reflect 20 % of all the radiation. To generalize the following equation:

$$L(T,\lambda) = \varepsilon(\lambda)L_{BB}(T,\lambda) \quad (16)$$

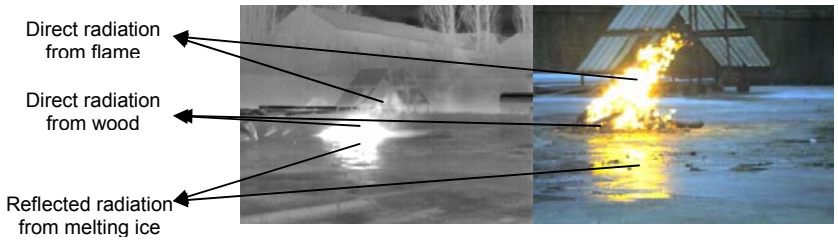

Figure 2: Reflection in the LWIR (left) and the Visible (right) wavelength bands

We must add a second term to account for the reflection.

$$L(T,\lambda) = \varepsilon(\lambda)L_{BB}(T,\lambda) + [1-\varepsilon(\lambda)]L_{BB}(T,\lambda) \quad (17)$$

This situation (Sun, Lamp…) could generate false alarms.

$$M_\lambda(\lambda,T,Q,F) = \int_{\lambda_1}^{\lambda_2} Q,F\frac{1-e^{-\alpha_\lambda d}}{\pi},\frac{2\pi c^2}{\lambda^5},\frac{1}{e^{\frac{hc}{\lambda kT}}-1}d\lambda + \int_{\lambda_1}^{\lambda_2} Q,F\frac{[1-(1-e^{-\alpha_\lambda d})]}{\pi},\frac{2\pi c^2}{\lambda^5},\frac{1}{e^{\frac{hc}{\lambda kT}}-1}d\lambda \quad (18)$$

2.5 Atmospheric Model

The radiation, leaving the fire, is different from the radiation, reaching the thermal detector by the attenuation of the atmosphere.

The in-band transmission τ_{atm}, depending on the fire range, is approximated by the Beer Lambert law.

$$\tau_{atm}(R,\lambda) = \tau_{atm}^{R}(\lambda) = e^{-\alpha(\lambda)R} \qquad (19)$$

R is the path length expressed in km and the extinction coefficient is expressed in km^{-1}.

This model gives a reasonable approximation if the waveband is large enough (Modtran is a better model).

$$M_b(\lambda_1,T,\Omega,F) = \int_{\lambda_1}^{\lambda_2} e^{-\alpha(\lambda)R}\,\Omega_s F(R)\frac{1-e^{-\alpha_s t}}{\pi}\,\frac{2\pi c^2}{\lambda^5}\,\frac{1}{e^{\frac{c_2}{\lambda T}}-1}\,d\lambda + \int_{\lambda_1}^{\lambda_2} e^{-\alpha(\lambda)R}\,\Omega_s F(R)\frac{\left[1-(1-e^{-\alpha_s t})\right]}{\pi}\,\frac{2\pi c^2}{\lambda^5}\,\frac{1}{e^{\frac{c_2}{\lambda T}}-1}\,d\lambda \qquad (20)$$

If the waveband is narrow, we need a more precise model taking into account the absorption, the emission and the scattering of the radiation.

2.6 Fire and Background separation model

Wildfire appears predominately as a 1000 K blackbody. The fire temperature varies between 700 K and 1500 K. The objective is to estimate by calculation, the ratio (contrast or separation) between the fire (radiation) and the background (radiation, reflectance).

In the Visible and SWIR bands, the background is modelled by the reflection of the sun, and the flame of the fire is modelled with Planck's law. In the LWIR, the background (earth temperature around 300K) and the fire is modelled with Planck's law. In the MWIR, the background is modelled by the sun reflection and the heat radiation (the ratio should be adapted depending on the bandwidth of the wavelength) and the flame of the fire is modelled by Planckian fire emission. Based on the results described in the table, we notice that the MWIR band has the biggest contrast between the fire radiation (1000 K) and the background (radiation and sun reflection), even at low fire temperature. The disadvantage of this waveband is the price and reliability. The MWIR InSb detector must be cooled (low dark current) in order to reach good results.

Table 1:Power densities of Fire and Background, including ratios, separation or contrast

Wavelength Band	Fire Temperature				Background Reflection or Radiation
	1500 K	1200 K	1000 K	700 K	
Visible Fire W/m^2 [0.4-0.7 µm]	160	4	0.1	0	Sun reflection in visible
Visible: Ratio Fire/Sun Reflec.	0.16	0.004	0.0001	0	1000 W/m^2
SWIR Fire W/m^2 [0.9-1.7 µm]	47824	8521	1617	27	Sun reflection in SWIR
SWIR: Ratio Fire/Sun Reflec.	160	28	5	0.1	300 W/m^2 (sunny day, not specular)
MWIR Fire W/m^2 [3-5 µm]	77575	39327	20462	4088	300 K background temperature
MWIR: Ratio Fire/Background	2585	1310	682	136	6 W/m^2 Rad. + 24 W/m^2
LWIR: [8-12 µm]	10265	7063	5038	2317	300 K background temperature
LWIR: Ratio Fire/Background	85	58	41	19	121 W/m^2

The LWIR also has a very good fire radiation and background radiation difference. The advantage here is that we have an uncooled [8-12 µm] micro-bolometer. The price is in general lower compared to the cooled photodiodes detectors. We saw that the dynamic in terms of the SNR of the signal is around 1000 of the µBolometer. The integration time could be changed between 10 to 60 µs (one video line). In practice, we calibrate the thermal camera for thermography with 3 different integration times. With an integration time Tint = 60 µs, the temperature range varies between -20 degrees to 120 degrees. With an integration time Tint=30 µs, the temperature range varies between 0 degree to 200 degrees. With an integration time Tint=10 µs, the temperature range varies between 30 degrees to 400 degrees. During the recordings, we used an integration time of 60 µs. This allowed us to see the background which could be useful information for the operators.

The SWIR also has a good fire radiation and background radiation difference. It is very effective for high fire temperature. The advantage here is that we have an uncooled InGaAs camera. The price is in general lower compared to the cooled photodiodes detectors. The SWIR camera signal dynamic is around 1000 and the integration time varies between 1 to 1000 µs. High signal dynamic increases the separation of the background radiance and the fire radiance. Background and fire radiance can overlap if dynamic is low, if MTF is low and if range is far (atmospheric attenuation eq. 21 and emissivity decrease with angle eq. 22). The dynamic and the MTF (Modulation Transfer Function) parameters are now optimized for fire detection.

3. ELECTRO-OPTICAL SYSTEM ANALYSIS

The collected signal depends mainly on the optical parameters (FL, F/#) and the type of detectors (LWIR uncooled micro-bolometer, MWIR InSb detector, SWIR InGaAs detector, Visible CMOS or CCD detectors).
The fire detection range estimation is based mainly on two parameters, the sensitivity and the spatial / angular resolution. If the temperature variation ΔT is small, sensitivity is the main parameter [6]:

$$SNR = \frac{\Delta T \cdot e^{-\gamma(\lambda)R}}{NETD} \quad (21)$$

If the temperature between the fire and the background is large, resolution is the main parameter.

$$Range = \frac{Object}{\#pixels \frac{pitch}{f}} = \frac{Object}{\#pixels IFOV} = \frac{Object}{\vartheta_{resolution}} \quad (22)$$

Smoke and flame modeling of the fire remains a challenging problem. We will consider here a limited number of features or parameters for the electro-optical analysis. The SWIR or LWIR infrared cameras detect only the heat flux. Smoke is not detected in the infrared. The hot blob segmentation is based on a histogram threshold and an optimized integration time at the read out level of the image detector.

Two pixels at least are necessary for hot blob detection. The hot blob criterion is not always enough in order to discard the false alarms generated by the sun, the lamps or hot spots. We selected the Johnson criteria to define the fire detection (2 pixels @ 100%), recognition (8 pixels @ 100%) or identification (15 pixels @ 50%). The fire detection range is also defined by the size of the fire. If the size of the flame is 1 m^2, 5 m^2 or 20 m^2, we will have C_{min}=sqrt(1)=1, C_{min}=sqrt(5)=2.23 and C_{min}=sqrt(20)=4.47.

Table 2 Detection range function of the detector, the lens and the fire size for an uncoooled LWIR camera

FLAME									
Camera	**LWIR Gobi 384, 284x288, 25 um pitch**								
Focal Length	**25 mm**			**100 mm**			**150 mm**		
HFOV	21.8 °			5.5 °			3.7 °		
VFOV	16.4 °			4.1 °			2.7 °		
IFOV	1 mrad			0.25 mrad			0.17 mrad		
Flame Size	1 m^2	5 m^2	25 m^2	1 m^2	5 m^2	25 m^2	1 m^2	5 m^2	25 m^2
Detection Range	500m	1115m	2235m	2000m	4460m	8940m	3000m	6690m	13410m
Recogn. Range	125m	278m	558m	500m	1115m	2235m	750m	1672m	3352m
Identific. Range	83m	185m	372m	333m	743m	1490m	500m	1115m	2235m

Table 3: Detection range function of the detector, the lens and the fire size for a typical cooled MWIR camera.

FLAME	
Camera	**Onca MWIR InSb, 640x512 pixels, 15 um pitch, NETD < 20 mK, 14 bits Dynamic, Tint:10-**

	10000us								
Focal Length	**30 mm**			**330 mm**			**660 mm**		
HFOV	18.2 °			1.67 °			3.7 °		
VFOV	14.6 °			1.3 °			2.7 °		
IFOV	0.5 mrad			0.045 mrad			0.17 mrad		
Flame Size	1 m^2	5 m^2	25 m^2	1 m^2	5 m^2	25 m^2	1 m^2	5 m^2	25 m^2
Detection Range	1000m	2230m	4470m	11000m	24530m	49170m	22000m	49060m	98340m
Recogn. Range	250m	557m	1117m	2750m	6132m	12292m	5500m	12265m	24585m
Identific. Range	166m	371m	745m	1833m	4088m	8195m	3666m	8176m	16390m

Based on the following recorded image, we estimate the surface size of the generated smoke from a 1 m^2 flame fire. One square meter fire produces 100 m^2 smoke. If the size of the smoke is 100 m^2, we will have C_{min}=sqrt(100)=10.

Figure 5: Typical visible of a starting fire in the marine mountains near to the Turkish coast.

If the visible camera is mounted on the pan and tilt installed on a mast, the camera with a 50 mm lens can rotate 360 degrees and stop each 7 degrees for automatic fire detection image analysis. The smoke identification range reaches 10 km. With a 100 mm lens we could reach 20 km with good visibility conditions.

Table 4: Detection range function of the detector, the lens and the smoke size

	SMOKE			
Camera	**Color Visible IQeye 1600 x 1200 pixels, 4 um pitch**			
Focal Length [mm]	**16 mm**	**25 mm**	**50 mm**	**100 mm**
HFOV [degrees]	22.6 °	14.6 °	7.3 °	3.6 °
VFOV [degrees]	17.1 °	11 °	5.5 °	2.7 °
IFOV [mRad]	0.25 mRad	0.16 mRad	0.08 mRad	0.04 mRad
Smoke Size [m^2]	100 m^2	100 m^2	100 m^2	100 m^2
Identification Range [m]	3333 m	5200 m	10416 m	20833 m

The target signal (fire) is expressed differently if we have an extended target or a sub pixel target. The detection range depends on the signal and the noise. The example hereunder is selected for a photo detector.
Extended target:

$$Signal_{ext} = \int_{\lambda_1}^{\lambda_2} A_{pi}\,\tau_{int}\,QE\,\Omega_{sys}\,\frac{\left(\varepsilon_{fg}L_{BB}(T_{fg},\lambda) - \varepsilon_{bg}L_{BB}(T_{bg},\lambda)\right)}{E_p(\lambda)}\chi(\lambda)\tau_{opt}(\lambda)\tau_{atm}(R,\lambda)d\lambda \qquad (23)$$

$$\tau_{opt} = \tau_l(\lambda) + \tau_f(\lambda) + \tau_{ir}(\lambda) \qquad (26)$$

A_d detector area, t_{int} integration time, QE quantum efficiency, Ω_{sys} system solid angle, $\chi(\lambda)$ optical filter, $\tau_{opt}(\lambda)$ optical transmission, $\tau_l(\lambda)$: lens transmission, $\tau_f(\lambda)$: filter transmission, $\tau_w(\lambda)$: window transmission ,$\tau_{atm}(\lambda)$ attenuation transmission, E_p is the photon energy.
Sub pixel target:

$$Signal_{sub} = \int_{\lambda_1}^{\lambda_2} EOD \cdot \tau_{int} \cdot QE \cdot \Omega_{receiver} \cdot \frac{L_{TS}(\lambda)}{E_p(\lambda)} \cdot \chi(\lambda) \cdot \tau_{opt}(\lambda) \cdot \tau_{atm}(R,\lambda) \cdot d\lambda \quad (26)$$

EOD is the Energy On Detector.
The temporal noise model includes the photon noise due to the background scene, the optics, the cold shield if available, the detector noise, the readout noise and the A/D noise of the camera. The temporal noise is added to the spatial noise. From the signal and noise estimation, the signal to noise ratio is calculated in function of the range. The range also depends on the geometrical parameters (IFOV, FL, F#). This defines the desired detection range based on the fire size.

$$noise_{total} = \sqrt{noise_{temporal}^2 + noise_{spatial}^2} \quad (28)$$

The SNR is:

$$SNR = \frac{signal\_extended}{Noise\_total} \text{ or } SNR = \frac{signal\_subpixel}{Noise\_total} \quad (27)$$

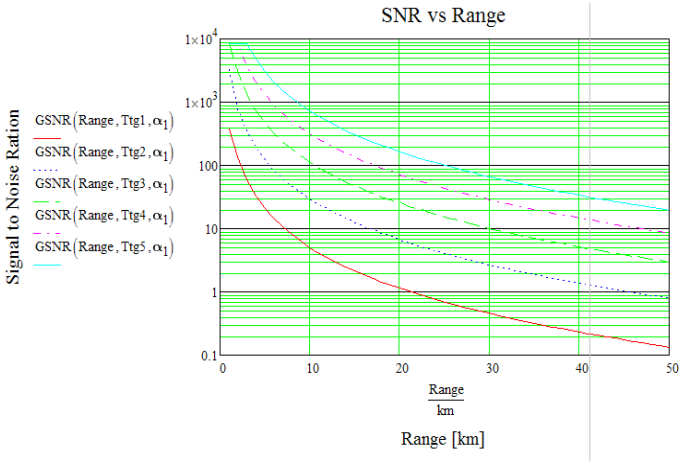

Figure 6: Signal to noise versus Range for 4 different temperatures

4. ELECTRO-OPTICAL SYSTEMS USED FOR THE FIRE DETECTION TRIALS

Three early fire electro-optical imaging detection systems were designed and tested for short and medium ranges during the FP-7 FIRESENSE project. The detection range of the fire (flame and smoke) is related to the detector, the optics and the atmospheric conditions.

The *Meerkat Fusion* (Visible color, SWIR and LWIR cameras) was designed for short ranges fire detection till 500 meters. The system includes a Visible CMOS Color camera, a Bobcat-1.7-320 InGaAs SWIR camera and a Gobi-384 LWIR micro bolometer camera. The optics has a focal length varying from 18 mm till 25 mm.

Figure 7: Meerkat Fusion

Figure 8: Meerkat PTZ with color visible and LWIR uBolometer camera

The *Meerkat PTZ* was designed for medium ranges fire detection till 5000 till 10000 meters. It includes a Gobi-384 LWIR µBolometer camera with a 15-100 mm zoom lens, a Bobcat-320 SWIR InGaAs camera and a CMOS color camera.

A prototype was designed for long range fire detection. The system includes a Onca-MWIR-InSb-640 camera with a 15-330 mm zoom lens and a Bobcat-1.7-320 SWIR InGaAs camera with a 75-300 mm lens.

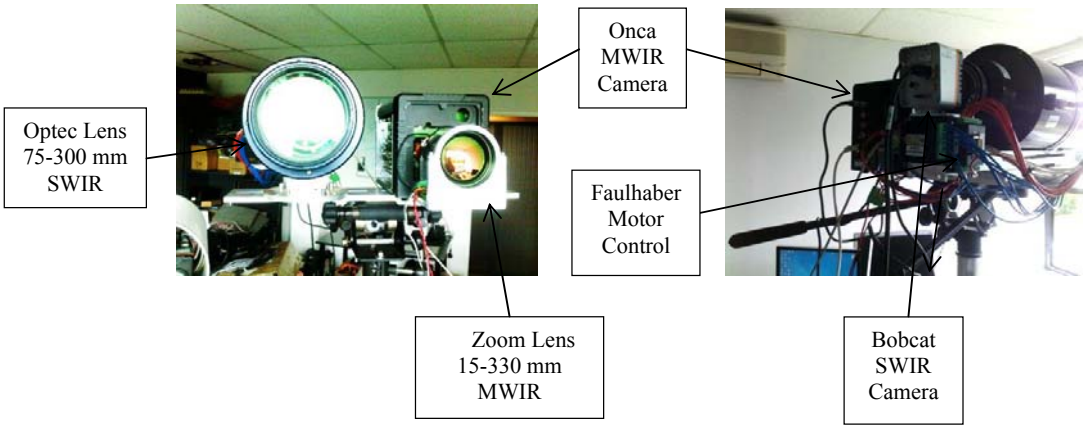

Figure 9: MWIR and SWIR cameras and lenses

5. IMAGE PROCESSING AND COMPUTER VISION FOR FIRE DETECTION

5.1 Image processing and computer vision contribution

There are mainly 3 different approaches to manipulate the pixels. The *image processing* processes the input pixels from the camera and results in processed pixels. The output is an enhanced image, a restored image, compressed image or a fused image. In *computer vision*, we extract information through a descriptor and convert the pixels in a symbol. Signal processing, pattern recognition and machine learning are some of the tools realizing the numerical to symbolic conversion. In *computer graphics*, we go from symbol or descriptor to the pixel. We will find nowadays the same classification and trend in the image application processors. The image processors includes specialized processors for image compression and image enhancement, specialized processors for computer vision as well as 2D and 3 D computer graphics.

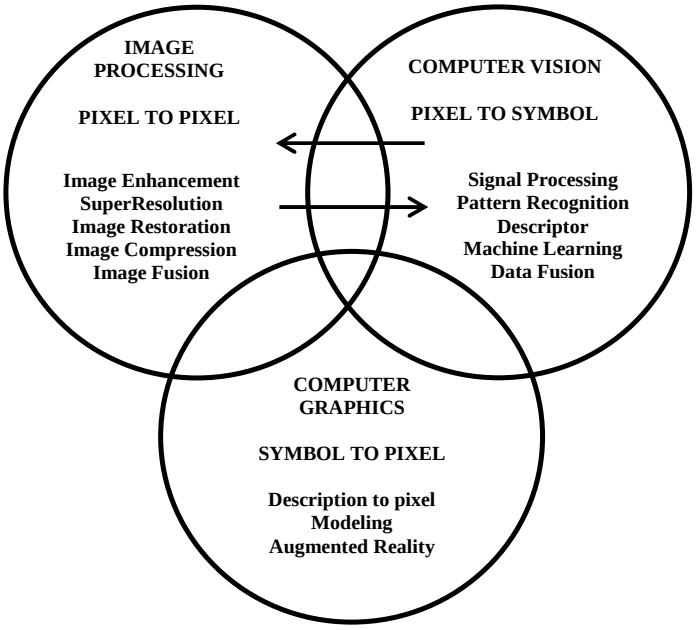

Figure 10: Image processing, Computer Vision and Computer Graphics contribution

We will focus here on the image processing and on the computer vision aspects. Image fusion and image enhancement techniques will be optimized for the operator in function of the mission. Providing the best image to the operator with events salient to the task will help him to confirm or deny the presence of a fire. Saliency, novelty, anomaly, attention and labeling could be enhanced with the computer graphic possibilities. The computer vision processing will detect automatically the fire. Computer vision principles are used in image fusion in order to improve the saliency of the flame and the smoke from different wavebands. Recognition of flame or smoke features (heat, movement, disorder characterization) will be salient events that are integrated in the fused image. The features and events that are novel or anomalous will trigger appropriate responses.

5.2 Camera settings optimization

The setting of the cameras (Integration time or exposure, shutter, focus, biasing, …) will be specific in function of the type of image processing and the type of computer vision. The main parameters of the cameras are the focus, the integration time and the iris. The setting of the parameters will define the histogram profile. For the operator the image should not be too dark or too saturated. The optimal setting will provide the optimal image information in function of the

mission. The global histogram analysis for example defines the appropriate camera parameters and provides a good signal to noise without any saturation.

In computer vision the camera parameters will depend on the pattern recognition method and the camera waveband. Hot blob detection from fire is optimal if the integration time of the LWIR and the SWIR is reduced. The intensity difference between the fire and the background is in practice high. This variability is increased with the detection range of the fire. The video receiver and the analog to digital converter have limited dynamic. The only way to avoid an overlap of the radiation histogram modalities will be the integration time and having a sharp focus. These parameters can be fixed or controlled automatically. After the appropriate settings, we are able to extract the hot blobs or highest temperature objects. The false alarms can still be generated by the sun, the reflection or by lamps. Feature disorder analysis will help us to reduce the false alarms.

Texture analysis (wavelets, covariance descriptor) of the smoke and flame requires specific settings. The global histogram should be set 20 % from the maximum histogram values. The figure hereunder describes the main camera parameters settings in function of the selected algorithms principles.

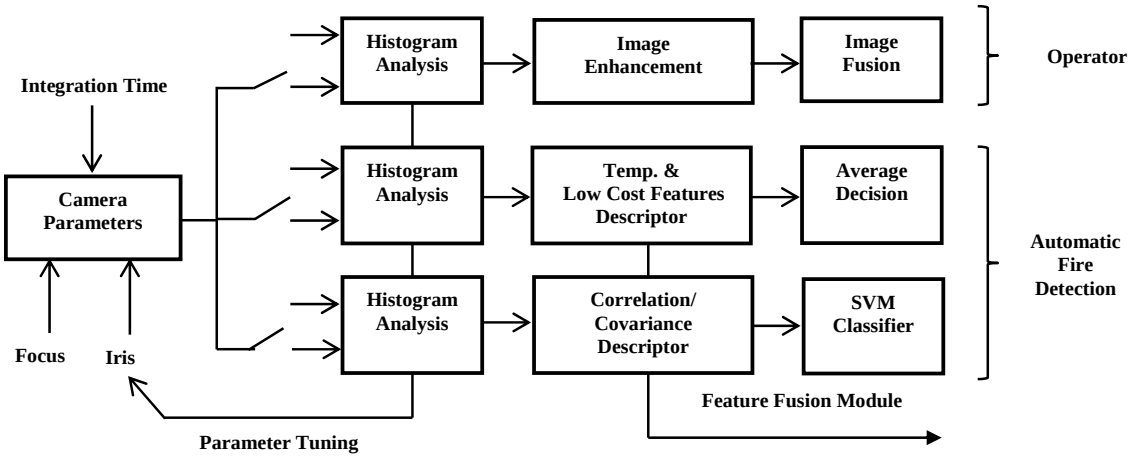

Figure 10: Camera Parameter Set Up

5.3 Automatic Fire Detection

Various principles and architectures with a large set of methods are available in image processing (pre-processing, segmentation, blob extraction), in pattern recognition (feature extraction, classical classification) and in machine learning (Deep Learning, Shallow Learning). Deep architectures (Convolutional Network, Deep Belief Nets) described in [22] include the low level features extractions that are combined progressively into more complex representation resulting in the learned classified output. This model should be able to capture and represent the knowledge from the pixels. Shallow architectures consist of an input layer transforming the raw input features into a specific feature space and an output layer. During the FireSense project the Support Vector Machine (SVM), using a Radius Basis Function (RBF) kernel was selected as one of the best available shallow method classifiers.

Different feature extraction methods, allowing dimension reduction, were selected to detect fire in the visible and the infrared band. In [16], the covariance descriptors are modeling the color, the spatial (including first and second derivative of intensity in x and y) and temporal (first and second derivative of intensity in time) information of the flame into a feature vector from image blocks. This method does not require background subtraction to segment moving region. This is a practical advantage. With the same method described in [17], the spatio-temporal correlation descriptor is modeling the smoke. The second method described in [18] is extracting color, contour, spatial and temporal variation features from the blobs extracted with a background subtraction method. The previous methods, using shallow methods, require expert

human knowledge, good data selection for the training and the test, extensive supervised training on labeled data and computational costs.

The objective of the last proposed method from [19] was to reduce the previous described drawbacks. Furthermore it will provide us with more insight concerning the results of the robust computational low cost features. Due to the specificity of the flame and the smoke, all the features of the fire hereunder are based on the disorder analysis.

Visible smoke and flame detection [19]

The dynamic background subtraction extracts the moving objects, and the temporal filtering removes objects which are not detected over multiple frames. The selected foreground (FG) objects in the video images are then further analyzed with three different flame disorder feature extractors: the bounding box disorder (BBD), the principal orientation disorder (POD) and the flame color rate (FCR).

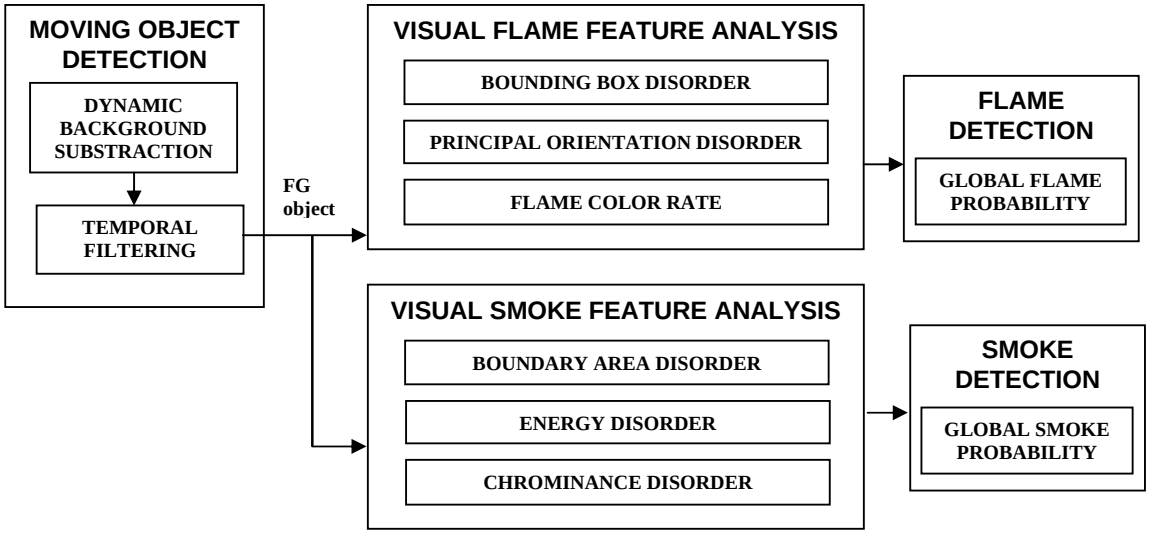

Figure 11: Low cost visible fire/smoke detection

The low cost smoke feature analysis is similar to the low cost flame feature analysis. The BBD and the POD algorithms are the same. The temporal disorder analysis of the area and perimeter of the smoke called bound area roughness (BAR) is added. The boundary area disorder (BAD) estimated from the BAR is calculated in the same way as the flame BBD and POD features. The energy disorder (ED) feature of the smoke is estimated with the discrete wavelet transform (DWT). A third feature estimates the chrominance disorder (CD) of the smoke. See [19].

Infrared flame detection [19]

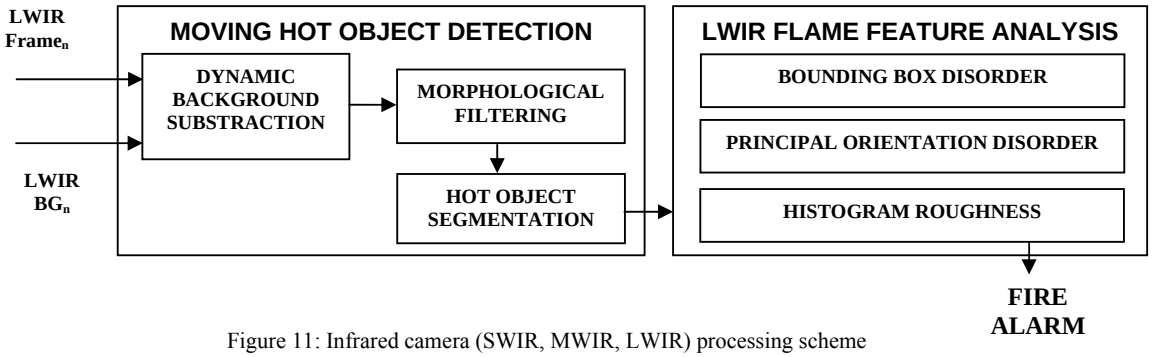

Figure 11: Infrared camera (SWIR, MWIR, LWIR) processing scheme

The moving flame is detected with a dynamic background subtraction and morphological filtering. The hot objects are extracted from histogram segmentation with the Otsu method [20].

In LWIR, MWIR and SWIR wavebands, the BBD and the POD flame feature analysis are equivalent to the visual features. The histogram roughness HR is the third added feature. The parameter of the automatic fire detector should be adjusted in function of the environment and the waveband.

The system will be tested with the Meerkat Fusion integrating 3 different wavebands (Visible, SWIR and LWIR) and a PC. Data transfer and command&control is executed over Gigabit Ethernet. All the processes are running on an Intel® Core™ i5-2540M CPU @ 2.6 GHz with 4 Gbytes installed RAM.

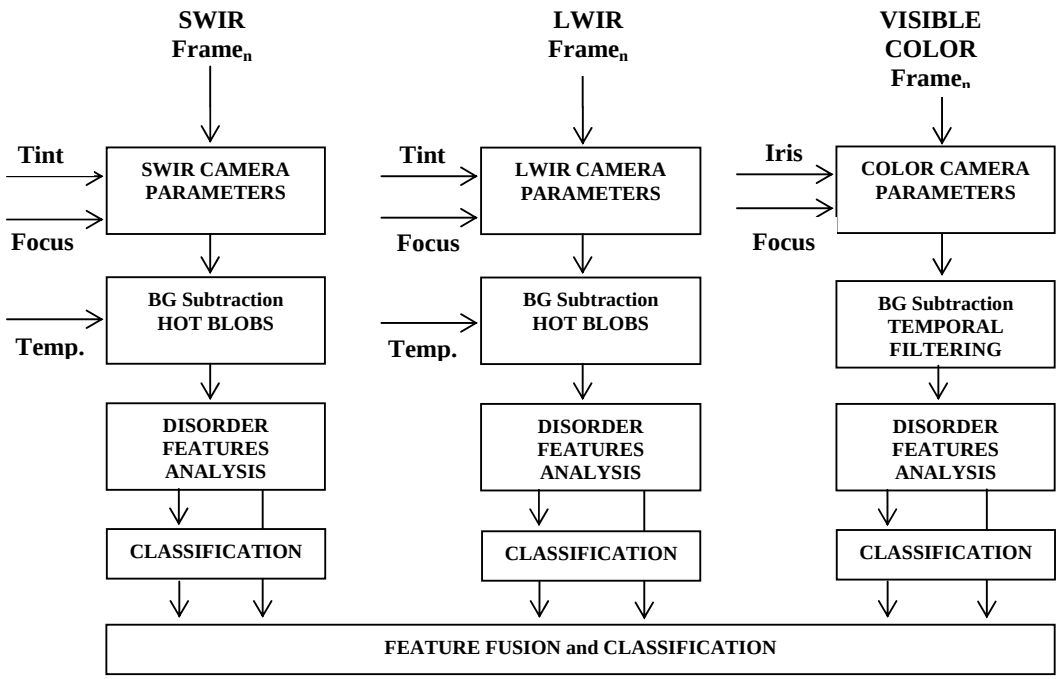

Figure 11: Infrared camera (SWIR, MWIR, LWIR) processing scheme

Each camera will provide his classification results by combining these different features and applying a threshold:

$$P^{visual}_{flame} = \frac{BBD + POD + FCR}{3} \qquad t^{visual}_{flame} = 0.7$$

$$P^{visual}_{smoke} = \frac{BAD + ED + CD}{3} \qquad t^{visual}_{smoke} = 0.7$$

$$P^{SWIR}_{flame} = \frac{BBD + POD + HR}{3} \qquad t^{SWIR}_{flame} = 0.7$$

$$P^{SWIR}_{flame} = \frac{BBD + POD + HR}{3} \qquad t^{SWIR}_{flame} = 0.7$$

If the risk value P^{SWIR} of an object exceeds the threshold t^{SWIR}, the frame in which it appears is labeled as fire.

Depending on the fire, the background and the waveband, one feature can be more discriminative than the other. This file, generated by each camera, will be provided to the data fusion module. The feature could be combined with several methods. More recordings and further researches on the feature fusion are needed.

Table 5: Table providing features analysis results of each blob in the frame

FRAME	CAM	BLOB	X	Y	WIDTH	HEIGHT	BBD	POD	HR	MCD	BED	Bilk. Pd	Gent Pd
319	2	1	238	202	24	3	0,2	0,2	0,2	0,6	0,2	0,3	0,2
320	2	1	238	202	24	3	0,4	0,2	1	0,5	0,4	0,375	0,53
321	2	1	234	202	25	3	0,3	0,2	0,8	0,6	0,3	0,35	0,43
322	2	1	234	202	25	3	0,4	0,6	0,6	0,5	0,2	0,425	0,53

5.4 Line Based Registration and Fusion of Images from IR and Vis Cameras

We have explored another edge-dependent registration algorithm that focuses on identifying matching linear structures in images produced by the different cameras. If we assume that the parallax can be controlled (e.g. by the use of a beam-splitter) or distances to objects in the scene are relatively large, we can with a first approximation use a projective transformation to model the changes between the images from different cameras. Since duality in 2-dimensional projective geometry ensures us that points and straight lines play an equivalent role, it follows that transformation parameters can equally be estimated by identifying corresponding lines. Compared to the traditional point-based approach, this process enjoys a higher robustness since lines (based on extracted edges) integrate information over a certain spatial extent and are therefore more reliably identifiable, even if the contrast polarity has been reversed. In fact, it is straightforward to formulate a unified framework in which point- as well as line-matches are treated on an equal footing. This is fortuitous as it significantly increases the amount of information that can be used to establish an accurate registration (For more details we refer to J. Han et al. [22] and [23]).
The problem of occasional contrast-reversal between IR and Vis images also plays a role when it comes to selecting an appropriate image fusion methodology. Indeed, a typical multi-resolution fusion algorithm will decompose both input images into sets of approximation and detail coefficients, and then reconstitute a new image by judiciously selecting the most salient coefficient from the available information. In image pairs where IR and Vis data provide complementary information of comparable strength (as is the case when observing fire and smoke) this might give rise to a patchy fusion result where there is chaotic competition between the opposite contrast in the input images. For that reason we have opted to implement a modified, asymmetric fusion scheme (dubbed *iconic fusion* [22]) in which one of the two input images (usually the Vis image) is chosen to be the reference image, while the other acts as an auxiliary source of additional information. As a consequence, the resulting fused image is visually reminiscent of the reference image but includes details only apparent in the auxiliary image.

To accomplish the above (assuming that the images have been registered) we perform a multi-resolution decomposition on both the reference (iconic) and the auxiliary image, and then recombine detail and approximation coefficients using the following rules (applied to small neighborhoods of pixels):

- If the detail coefficients of one of both images (i.e. reference *or* auxiliary image) are significant whereas the corresponding detail coefficients in the other image are negligible, then the former detail coefficients are transferred to the fusion image;
- If the detail coefficients of the reference image show some geometric structure (e.g. edge) but this structure is more pronounced in the auxiliary image, then the coefficients of the latter are preserved, but the *signs are changed to conform with the sign of the coefficients in the reference image*! This modification ensures that the resulting contrast in the fusion image mirrors that of the reference image.
- When combining the approximation coefficients, we use a weighted averaging where the local weights of the reference or ancillary image are determined by the saliency of the neighborhoods under scrutiny in the input images (e.g. hot spots detected in IR).

Figure 11: Iconic fusion with the visible camera (smoke) and the swir camera (fire)

6. CONCLUSIONS

A short, medium and long range multi-band electro-optical system was developed in the project based on a physical and system analysis. The short range multiband system, called Meerkat Fusion, used visible color, SWIR and thermal images that are combined in order to obtain better flame detection results and fewer false alarms.

ACKOWLEDGEMENTS

This R & D work has received funding from the European Community's Seventh Framework Programme (under grant agreement no FP7-ENV-244088 "Fire Detection and Management through a Multi-Sensor Network for Protection of Cultural Heritage Areas from the risk of fire and Extreme Weather". Our partners involved in this project are CERTH-ITI Greece, Bilkent University Turkey, SUPCOM Tunisia, CWI Netherland, Bogacizi University Turkey, HMC Greece, Titan Turkey and CNR Italy.
We thank Bart Sette, technical director of Warrington Fire Gent (WFRGENT N.V. Ottergemsesteenweg, 711, 9000 GENT, Belgium), who allowed us to use the facilities.

REFERENCES

[1] Vytenis Babrauskas Ph.D, [Ignition of wood a review of the state of the art.], Interscience Communications Ltd., London, 71-88 (2001).
[2] Georges W. Mulholland, [Smoke production and properties], SFPE Handbook of Fire Protection Engineering, 2nd Edition, Chapter 15, Section 2.
[3] E. Pastor, A. Rigueiro, L. Zarate, A. Gimenez, J. Adalmos and E. Planas, [Experimental methodology for characterizing flame emissivity of small forest fires using infrared thermography techniques], Forest Fire Research & Wildland Fire Safety, Viegas (ed.), (2002).
[4] Ambrose E. Ononye, Antony Vodacek and Robert Kremens, "Fire Temperature Retrieval using constrained spectral unmixing and emissivity estimation", SPIE Vol.5806 (2005).
[5] Peter Saunders, [Radiation Thermometry], Fundamentals and Applications in Petrochemical Industry, SPIE Press, (2007).
[6] Gerald C. Holst, [Electro-Optical Imaging System Performance], SPIE Optical Engineering Press, (2006).
[7] William Wam, "Passive IR Sensor Performance Analysis using Mathcad Modeling".
[8] Bradly J. Cooke, Bryan E. Laubscher and Christoph C. Borel, "Methodology for Rapid Infrared Multi-Spectral, Electro-Optical Imaging System Performance Analysis and Synthesis", SPIE Vol. 2743, (1996).
[9] Bart Merci. "Fire Safety Engineering. Fire Safety and Explosion Safety in Car Parks", http://www.carparkfiresafety.be/
[10] Steven Verstockt, Alexander Vanoosthuyse, Sofie Van Hoecke, Peter Lambert, and Rik Van de Walle, "Multi-sensor Fire Detection by Fusing Visual and Non visual Flame Features", Springer-Verlag Berlin Heidelberg (2010). Image and Signal Processing. 4th International Conference, ICISP 2010, Trois-Rivieres, QC, Canada, (2010)
[11] MF Audier, "Formation, capture et restitution des images", Course ESE22, (2009).
[12] Steven Verstockt, Charles-Frederik J. Hollemeersch, Chris Poppe, Peter Lambert, Rik Van de Walle, Sofie Van Hoecke, Bart Merci, and Bart Sette, "Multi-sensor fire detection by fusing visual and LWIR flame feature", ICGST International Journal on Graphics, and Image Processing 10(6), 43–50 (2010).
[13] Steven Verstockt, Chris Poppe, Pieterjan De Potter, Sofie Van Hoecke, Charles-Frederik J. Hollemeersch, Peter Lambert, and Rik Van deWalle, "Silhouette coverage analysis for multi-modal video surveillance", Proc. 29th Progress In Electromagnetics Research Symposium, 1279–1283 (2011).
[14] Kosmas Dimitropoulos, Kivanc Kose, Nikos Gammalidis and Enis Cetin, "Fire detection and 3D fire propagation estimation for the protection of cultural heritage areas".
[15] Toreyin B.U, [Fire Detection Algorithms Using Multimodal Signal and Image Analysis], PhD thesis Bilkent University, Department of Electrical and Electronics Engineering, Ankara-Turkey (2009).
[16] Yusuf Hakan Habiboglu, Osman Gunay and Enis Cetin, "Covariance matrix based fire and flame detection method in video", Machine Vision and Applications (2011).
[17] Y. Hakan Habiboglu, Osman Gunay and Enis Cetin, "Real time wildfire detection using correlation descriptors", 19th European Signal Processing - EUSIPCO 2011, (2011)
[18] KosmasDimitropoulos, Filareti Tsalakanidou and Nikos Grammalidis, [Video based flame detection, using spatiotemporal features and SVM Classification], Informatics and Telematics Institute, CERTH.

[19] Steven Verstockt, [Multi-modal Video Analysis for Early Fire Detection], Phd Dissertation. Faculteit Ingenieurswetenschappen en Architectuur - Universiteit Gent (2012).
[20] N.Otsu, "A threshold selection method from grey level histograms", IEEE Transactions on Systems, Man and Cybernetics 9(1), 62-66 (1979).
[21] Jungong Han, Eric J. Pauwels and Paul de Zeeuw, "Visible and Infrared Image Registration in Man-Made Environments Employing Hybrid Visual Features", Pattern Recognition Letters-Special Issue On Multi-Spectrum Video Processing for Semantic Computing (announced)
[22] Paul M. de Zeeuw, Eric J. Pauwels and Jungong Han, "Multimodality and Multiresolution Image Fusion", Proc. VISAPP 2012: International Conference on Computer Vision Theory and Applications 1, 151 – 157 (2012).
[23] Yoshua Bengio, Yann LeCun, "Scaling Learning Algorithms toward AI". Internet.